Egusquiza, MG.; Soriano Rodríguez, MD.; Muñoz, M.; Romanelli, G.; Soriano-Rodríguez, J.; Cabello, CI.; López Nieto, JM. (2021). Precursors of tetragonal tungsten bronzes as catalysts in selective reactions: Liquid phase oxidation of diphenyl sulfide and gas phase oxidation of hydrogen sulfide. Catalysis Today. 372:70-81. https://doi.org/10.1016/j.cattod.2021.05.001

Precursors of tetragonal tungsten bronzes as catalysts in selective reactions: liquid phase oxidation of diphenyl sulfide and gas phase oxidation of hydrogen sulfide

by

María G. Egusquiza[a], M. Dolores Soriano[b], Mercedes Muñoz[a], Gustavo Romanelli[a], José Soriano[b], Carmen I. Cabello[a,c], José M. López Nieto[b]

[a] "Centro de Investigación y Desarrollo en Ciencias Aplicadas Dr. J.J. Ronco", CINDECA, CCT CONICET La Plata - Universidad Nacional de La Plata- CIC-PBA, Calle 47 No. 257, 1900 La Plata, Argentina. Email: megus@quimica.unlp.edu.ar

[b] Instituto de Tecnología Química, Universitat Politècnica de València-Consejo Superior de Investigaciones Científicas, Avenida de los Naranjos s/n, 46022 Valencia, Spain. Email: jmlopez@itq.upv.es

[c] CIC-PBA Researcher – Facultad de Ingeniería, UNLP, 1900, La Plata, Argentina. Email: ccabello@quimica.unlp.edu.ar

Abstract

Mixed metal oxides, of the type $(KNaM)_xP_{0.11}WV_{0.2}NbO_x$ and $(NH_4)_x/(Na)_xP_{0.11}WV_{0.2}NbO_x$, were prepared by hydrothermal synthesis from lacunary heteropolytungstates, $[M_4(H_2O)_2(PW_9O_{34})_2]^{10-}$ (MPW_9, with $M^{(II)}$ =Co, Cu or Mn) and their precursor $Na_8H(PW_9O_{34})$ ($NaPW_9$), chemically modified by $Nb^{(V)}$ and $V^{(IV)}$. For comparison mixed metal oxides were also synthesized by using a Keggin heteropolytungstates $[PW_{12}O_{40}]^{3-}$ as tungsten precursor. The pristine samples were finally heat-treated at 500 ºC in flowing N_2 for 2h. The resulting mixed metal oxides were characterized by several physico-chemical techniques and tested in both the liquid phase catalytic oxidation of diphenyl sulfide (DPS), in friendly environmental conditions (using *tert*-butyl hydroperoxide as oxidant), and in the gas phase partial oxidation of hydrogen sulfide to sulfur (using air at oxidant). Although the catalytic behavior of these catalysts strongly depends on the composition of catalysts, high activity and selectivity have been achieved over mixed metal oxides in both reactions. The good catalytic performance of species containing $Cu^{(II)}$ was evidenced in both reactions studied and the reactivity of this element could be explained by its structural and vibrational spectroscopic properties.

Keyword: hydrothermal synthesis, catalytic oxidation, diphenyl sulfide, hydrogen sulfide, environmentally friendly conditions.

1. INTRODUCTION

Many of the environmental laws are intended to limit the sulfide content in oil derivatives, such as diesel or fuel oil. In this respect, the hydrodesulfurization process of oil cuts that is used widely in the petrochemical industry requires high pressures and temperatures, great volume reactors, polluting reagents and long times of reaction, factors that turn it into an expensive process. An interesting alternative is the oxidative desulfurization (ODS) of the above-mentioned oil derivatives to sulfone and/or sulfoxide in friendly environmental conditions. Besides, this kind of reaction is relevant in the field of the pharmaceutical and food industries. In general, the catalytic oxidation of aromatic sulfides to sulfoxide has a lower conversion rate than that observed for the sulfoxide-sulfone process, which makes it difficult to synthesize medicines that require less than 0.5% of sulfones in their formulation (such as rabeprazole, lansoprazole, omeprazole, etc.). In this sense, the sulfoxide-sulfone separation process necessary for the isolation of active species must be optimized [1-7].

Recently, studies have been reported that allow oxidative desulfurization both in batch (at 80 ºC) and in fixed-bed reactors catalyzed by oxidic precursors of transition metals such as tungstates or molybdates that can be supported on γ-Al_2O_3, SiO_2 or W heteropolyanions [8-11]. Oxidants such as peroxides are oxygen carriers that produce nonpolluting residues and facilitate direct access to oxygen, and they are easy to store and of low cost. In our previous works about MoO_x/ZrO_2 systems, high conversion of DPS (88%) and selectivity to diphenyl sulfone ($DPSO_2$) (60%) was obtained for the pH 2 series of catalysts [12]. These results have suggested that the acid environment was the most efficient synthesis parameter leading to the formation of polymolybdate species which are considered the active phases in this reaction. Likewise, in a recent paper related to the use of ammonium heptamolybdate and heteropolymolybdates Anderson type

Al/$CoMo_6$ phases supported in metakaolin, it has been shown that the presence of sites with different characteristics, i.e. Brönsted/Lewis acid and redox sites, generate a bifunctional character favoring both the formation of peroxo intermediary molybdates and the subsequent nucleophilic attack of the sulfur atom in the sulfide by peroxo species [13]. In the same way, the existence of W intermediary peroxo species and its efficiency in this type of reactions has been proven. Thus, bi- or tetra-nuclear peroxo intermediate species facilitates the interaction of peroxo bonds with C–C bonds [14, 15].

The idea of carrying out the present work was inspired by taking into account our previous studies about the structural, spectroscopic and thermal properties of a series of lacunary heteropolytungstates of general formula, $K_{10}[M_4(H_2O)_2(PW_9O_{34})_2]\cdot 20H_2O$ (MPW_9) with $M=Co^{(II)}$, $Zn^{(II)}$, $Cu^{(II)}$ and $Mn^{(II)}$, and their precursor, $Na_8HPW_9O_{34}\cdot 19H_2O$ (NaPW9) [16]. An exhaustive analysis of its thermal stability in an oxidizing and reducing atmosphere revealed an interesting behavior that led us to test these phases as catalysts in several the selective oxidation reactions. The decomposition scheme of complex start-up phases is practically similar for different atmospheres. In oxidizing and inert atmosphere, the formation of K_xWO_3 type bronzes (800 ºC) is mostly observed, in reducing atmosphere K_xWO_3 bronzes are obtained between 600º and 700 ºC. Moreover, under these conditions, it was observed that the metal of the cluster affects the reducibility of $W^{(VI)}$ causing a decrease of 200 ºC in its reduction temperature, according to the following order Cu > Co > Mn coincident with the increase in the reducibility of the divalent metal or with the decreasing order of its redox potentials. On the other hand, the structural stability induced by the metal of the cluster, both in oxidizing or inert atmosphere as reductive, obeys the opposite order: PWCu < PWCo < PWMn. Reduction limitations of $W^{(VI)}$ present in the structure of these bronzes are improved by partially replacing it with

elements such as $Nb^{(V)}$ and $V^{(IV)}$ [16]. Thermal decomposition schemes (1 reducing and 2 air atmosphere) are shown in supplementary information.

Thus, these lacunary heteropolytungstates were studied in selective oxidation of DPS [11] and 2-naftol [17] and epoxidation of limonene [18]. As the $CuPW_9$ phase showed the best activity and selectivity in the oxidation of limonene, kinetic studies were carried out by changing the limonene / H_2O_2 / catalyst ratio. In addition, the $CuPW_9$ phase supported on alumina was evaluated as a heterogeneous catalyst [19]. Most of these results showed the highest reactivity of the Cu and Co compounds against the other members of the series. It has been suggested that the different behavior of the Cu phases could be related to the point asymmetry of the CuO_6 octahedra due to the Jahn-Teller effect [$Cu^{(II)}\, t_{2g}^6 e_g^3$]. It is known that some $Cu^{(II)}$ complexes present symmetrical CuO_6 structural sites at low temperature which are distorted (tetragonal symmetry) when temperature increases [20]. Particularly in the synthesis of the $CuPW_9$ phase, the product obtained is highly dependent on the experimental conditions such as time and temperature. Under the general recrystallization conditions for the derivatives of $Co^{(II)}$, $Zn^{(II)}$ and $Mn^{(II)}$ (100 °C, aqueous medium), an unidentified thermolysis product of $CuPW_9$ was obtained mostly, while if recrystallization was conducted at low temperature (<60ºC and short times) a better performance of the complex $[Cu_4(H_2O)_2(PW_9O_{34})_2]^{10-}$ was achieved. Later works identified the thermolysis product as the heteropolyoxotungstate of formula $[Cu_2(H_2O)_2PW_{10}O_{38}]^{7-}$ which occurs in the form of two isomers containing neighboring $Cu^{(II)}$ atoms in two different types of bonds (a) connected through oxygens from the vertices of the octahedra and (b) connected through the edges of their coordination octahedra, [17- 19, 20].

Regarding the preliminary work referred to the selective oxidation of DPS [11], it was observed that the activity of the MPW_9 systems compared with that of the precursor phase

$NaPW_9$ was related to the presence of the metal and particularly to the chemical properties. In this sense, the redox character of the divalent species, the stability of their oxidation state, the chemical affinity towards the reagent and the local M symmetry played an important role in defining the following order of activity $CuPW_9 > CoPW_9 > ZnPW_9 > MnPW_9 > NaPW_9$ [11]. The reactivity was in accordance with the redox potentials for the reduction couple $M^{(II)}/M$, $E^o\ Cu^{(II)}/Cu = 0.34 > E^o\ Co^{(II)}/Co = -0.28$ V $> E^o\ Zn^{(II)}/Zn = -0.76$ V $> E^o\ Mn^{(II)}/Mn = -1.03$ V [16], pointing out the lower copper capacity to remain as divalent species. Contrary, $Mn^{(II)}$ only presents higher oxidation states while $Co^{(II)}$-$Co^{(III)}$ oxidation is relatively difficult in absence of adequate environment. $Zn^{(II)}$ is inert to oxidize, whereas $Cu^{(II)}$ is the unique species easy to reduce to monovalent ion ($Cu^{(II)}/Cu^{(I)}$= 0.16 V). On the other hand, the asymmetry of CuO_6 polyhedra by Jahn Teller effect, responsible for the $CuPW_9$ instability, increases the interaction with the reactive and consequently the catalyst activity. Additionally, it was possible to suggest an increase of the Cu(I)-sulfide species according to the hard and soft Pearson' acids classification, which can favor the formation of an intermediate meta-stable phase [11].

Furthermore, the thermal analysis of MPW_9 and $NaPW_9$ in both oxidizing and reducing atmosphere showed the possibility of preparing mixed oxides as precursors to bronzes. The formation of $KxWO_3$ bronzes could be observed as the temperature increases (~800 ◦C) [16].

Other oxidic precursors of tungstates or molybdates, such as $WMo_{1-x}V_zO_z$ or $W_{1-x}Me_xO_z$ with bronze structure, show interesting results as catalysts in the gas phase partial oxidation of H_2S [21] and in the aerobic oxidative dehydration of glycerol to acrylic acid [22]. In these phases, part of the molybdenum or tungsten atoms have been isomorphically replaced by vanadium, molybdenum and/or niobium atoms. The best catalytic results

have been obtained for the tri-metallic catalysts, in particular those with a hexagonal tungsten bronzes (HTB) structure [22]. These catalysts, formed by hexagonal rings that host ammonium cations inside, present Brönsted/Lewis acidic sites after heat-treatments depending on the catalyst composition [21,22]. Nevertheless, the $W^{(VI)}$ ions are difficult to reduce. To correct these limitations, vanadium and/or molybdenum were introduced in these materials because of their high catalytic redox activity in partial oxidation reactions. $V^{(IV)}$, $Nb^{(V)}$ and/or $Mo^{(VI)}$ can isomorphically partially replace $W^{(VI)}$ ions in the hexagonal tungsten bronze structure [21, 22]. Likewise, some tetragonal tungsten bronzes (TTB), prepared hydrothermally from synthesis gels (aqueous solution of V- and Nb-precursors and from Keggin-type heteropolyacids), were used as catalysts in the gas phase partial oxidation of olefins, presenting high activity and selectivity [23]. In addition, semi-crystalline material (which could be considered as precursors of tetragonal tungsten bronze structures) have been also proposed as active and selective catalysts for the catalytic abatement of trichloroethylene [24].

In the present work, the lacunary Keggin complex ($NaPW_9$ and MPW_9 derivative with M = $Co^{(II)}$, $Cu^{(II)}$ and $Mn^{(II)}$) were chemically modified by $Nb^{(V)}$ and $V^{(IV)}$ by means of a hydrothermal synthesis, giving place to the formation of P-W-V-Nb-O and P-W-V-Nb-M-O solids, which can be considered as precursor oxides of tetragonal tungsten bronzes. For comparison, Keggin-derived heteropolyoxotungstates and the corresponding P-W-V-Nb-O metal oxides were also prepared.

According to the literature and our previous studies, we decided to test the catalytic potential of the mentioned mixed oxides arising from the hydrothermal treatment of Keggin-derived heteropolyoxotungstates. All catalysts were characterized and tested in both the liquid phase selective oxidation of DPS, in environmentally friendly conditions

and using *tert*-butyl hydroperoxide (TBHP) as oxidant, and in the gas phase partial oxidation of H_2S to sulfur, using air as oxidant.

2. EXPERIMENTAL

2.1. Preparation of catalysts

2.1.1. Preparation of heteropolytungstates

The synthesis and characterization of lacunary heteropolytungstates, i.e. $Na_8H(PW_9O_{34})$ (named as **$NaPW_9$**) and $[M_4(H_2O)_2(PW_9O_{34})_2]^{10-}$ (named as **MPW_9**, with $M^{(II)}$ = Co, Cu or Mn) have been reported previously [16, 17]. On the other hand, Na^+ cation of the lacunary Keggin $Na_8H(PW_9O_{34})$ phase was replaced by NH_4^+ by adding an excess of CH_3COONH_4 solid salt to an aqueous solution of the $NaPW_9$ and allowing it to crystallize. The pH was adjusted to 2 by the addition of glacial CH_3COOH. The resulting solution was filtered, and the solid was allowed to dry at room temperature (and named as **NH_4PW_9**).

For comparative purpose, some Keggin-derived phases, i.e. $(NH_4)_3PW_{12}O_{40}$ (named as **NH_4PW_{12}**), was prepared from polyoxotungstate $H_3PW_{12}O_{40}$ by adding an excess of NH_4HCO_3 solution to an aqueous solution of $H_3PW_{12}O_{40}$ under stirring at room temperature [25]. Sodium phosphotungstate, $Na_3PW_{12}O_{40}.xH_2O$ (Aldrich) was named as **$NaPW_{12}$** and used also as a reference.

2.1.2. Preparation of mixed metal oxide bronzes

Mixed tri- and tetrametallic oxides, i.e. P-W-V-Nb-O and M-P-W-V-Nb-O mixed oxides, were prepared hydrothermally (at 175 ºC for 48h) from aqueous solutions of vanadyl sulfate, niobium oxalate and Keggin heteropolytungstates (i.e. $NaPW_9$, NH_4PW_9, $NaPW_{12}$ or NH_4PW_{12}, but also from MPW_9; $M^{(II)}$= Cu, Co or Mn), according to a procedure similar to one previously reported [22, 24]. The resulting solids were washed with water, dried at 100 ºC in an oven. Finally, the solids were heat-treated in N_2 at 500 ºC for 2h.

Samples heat-treated at 500 ºC will be named as VNb-X and VNb-MX, in which X ($NaPW_9$, NH_4PW_9, $NaPW_{12}$ or NH_4PW_{12}) and MX ($CoPW_9$, $CuPW_9$ or $MnPW_9$) are the polyoxotungstate used in the hydrothermal synthesis.

2.2. Characterization of catalysts

The specific surface areas of the catalysts were obtained in an ASAP 2000 apparatus, using the BET method from the nitrogen adsorption isotherms. Samples were degassed in situ under vacuum at 250 ºC.

X-ray diffraction patterns (XRD) were collected using a Philips X'Pert equipped with a graphite monochromator operating at 40 kV and 45 mA and with Cu Kα Ni radiation filter (λ = 0.1542 nm).

Scanning electron microscopy (SEM-EDS) performed under a Philips 505 microscope equipped with EDAX 9100 microprobe. In this work no microphotographs are shown and only Energy Dispersive Spectroscopy was used to perform a semi-quantitative analysis of the elements.

Infrared spectra were recorded at room temperature in the 300–4000 cm^{-1} region with a Nicolet 205xB spectrophotometer equipped with a data station at a spectral resolution of 1 cm^{-1} (accumulations of 128 scans).

Raman spectra were recorded in ambient conditions using an "in via" Renishaw spectrometer, equipped with an Olympus microscope, at an exciting wavelength of 514 nm (a Renishaw HPNIR laser power of approximately 15 mW).

Diffuse reflectance UV–vis (DR–UV–vis) spectra were recorded on a Cary 5 equipped with a Praying Mantis attachment from Harric.

2.3. Catalytic evaluation

Heteropolyoxometalates and mixed metal oxides bronzes (heat-treated at 500 ºC) were tested in two different reactions: i) The liquid phase selective oxidation of DPS, using TBHP as oxidant; and ii) The gas phase partial oxidation of hydrogen sulfide, using oxygen as oxidant.

2.3.1. Catalytic tests in the selective oxidation of DPS

The catalytic test for the liquid phase selective oxidation of DPS was carried out in batch at 80 ºC, under magnetic stirring at 800 rpm, using 1mmol% of the catalyst in 5 ml of toluene, 1 ml of TBHP (5M) and 1 mmol of DPS. Aliquots were taken at different time intervals. Prior thin layer chromatography (TLC) monitoring was done with a mixture of hexane: ethyl acetate (5:1). Reactant and reaction products were quantified by gas

chromatography in a Shimadzu 2014 instrument fitted with a 30 m × 0.32 mm SPB-1 capillary column and equipped with a FID detector [10].

Turnover number (TON) was calculated by dividing the number of molecules obtained per number of catalyst molecules used in the reaction. And we calculated turnover frequencies (TOF) dividing the number of molecules of product obtained per number of catalyst molecules used in the reaction in time unit (min).

$$TON = \frac{n_{\,product} \times X}{n_{catalyst}}$$

$$TOF\ (min^{-1}) = \frac{\left(\frac{n_{\,product} \times X}{n_{catalyst}}\right)}{time}$$

Where $n_{\,product}$ were the mmols of product obtained at 150 min of reaction, $n_{\,cataliyst}$ were the mmols of catalyst, *X* was the conversion at 150 min of reaction and *time* was reaction time.

2.3.2. Gas phase partial oxidation of hydrogen sulfide

The gas phase partial oxidation of hydrogen sulfide (H_2S) was carried out, at atmospheric pressure, in a tubular quartz reactor with fixed bed flow at 180 ºC using 100 mg of catalyst and a flow rate of 130 ml min^{-1} (using a H_2S/air/He molar ratio of 1.2/5.0/93.8. Analysis of reactants and reaction products was carried out online by gas chromatography using two different chromatographic columns [21]: i) Molecular Sieve 5 A (for O_2 and N_2); and ii) Porapak T (for H_2S and SO_2).

3. RESULTS AND DISCUSSION

3.1. Characterization of catalysts

Table 1 shows the structure type, S_{BET} values and chemical analysis by SEM-EDS of both heteropolytungstates, i.e. $NaPW_9$, NH_4PW_9, $NaPW_{12}$, NH_4PW_{12} and MPW_9 ($M^{(II)}$= Co, Cu, Mn), and the corresponding mixed metal oxides, synthesized hydrothermally and heat-treated at 500 ºC in N_2 (i.e. VNb-X and VNb-MX series). Regarding the S_{BET} values, it is well known that iso and hetero polyoxocompounds are generally polycrystalline solids with surface areas less than 40 m^2/g. These values are considered negligible in relation to the S_{BET} of a heterogeneous catalyst, which is important above 100 m^2/g. As can be seen, the mixed oxides obtained by hydrothermal synthesis presented S_{BET} area values above such value, with the exception of the species containing $Co^{(II)}$ ($VNb\text{-}CoPW_9$ sample).

In this paper no microphotographs are shown, only EDS has been used to perform a semi-quantitative analysis of the elements.

Table 1.

Figure 1 shown the XRD patterns of starting Keggin heteropolytungstates ($NaPW_9$, NH_4PW_9, $NaPW_{12}$, NH_4PW_{12}), and the corresponding mixed metal oxides after heat-treatment at 500 ºC (VNb-X series). On the other hand, Figure 2 shows the XRD patterns of metal-containing polyoxometalates (MPW_9 series, with $M^{(II)}$= Co, Cu, Mn) as well as the XRD patterns of the corresponding mixed metal oxides heat-treated at 500 ºC (VNb-MX series).

For comparison, the solid achieved from hydrothermal synthesis, as-synthesized solids (as-VNb-X series and as-VNb-MX series), before heat-treatment, are also included in Figs. S1 and S2 (supplementary information), respectively.

The XRD patterns of heteropolyoxotungstates are in good agreement to those previously reported [16], and strongly depend on the composition of heteropolyacids.

On the other hand, the XRD patterns of solid achieved by hydrothermal synthesis and heat-treated at 500 ºC in a N_2 atmosphere, i.e. VNb-X series (Fig. 1) and VNb-PW_9 (Figs. 2), revealed that, independently of the polyoxotungstate used in the hydrothermal synthesis, produces a pseudo-crystalline material with an intense peak at ca. 2θ = 22.8° (interlaminar spacing of 3.9 Å).

As indicated previously, the incorporation of $V^{(IV)}$ and/or $Nb^{(V)}$ within the framework of these mixed metal oxides can favor a loss of log-range order in the ab plane, growing along the c axis (peak at 2θ= 23º) [23, 24].

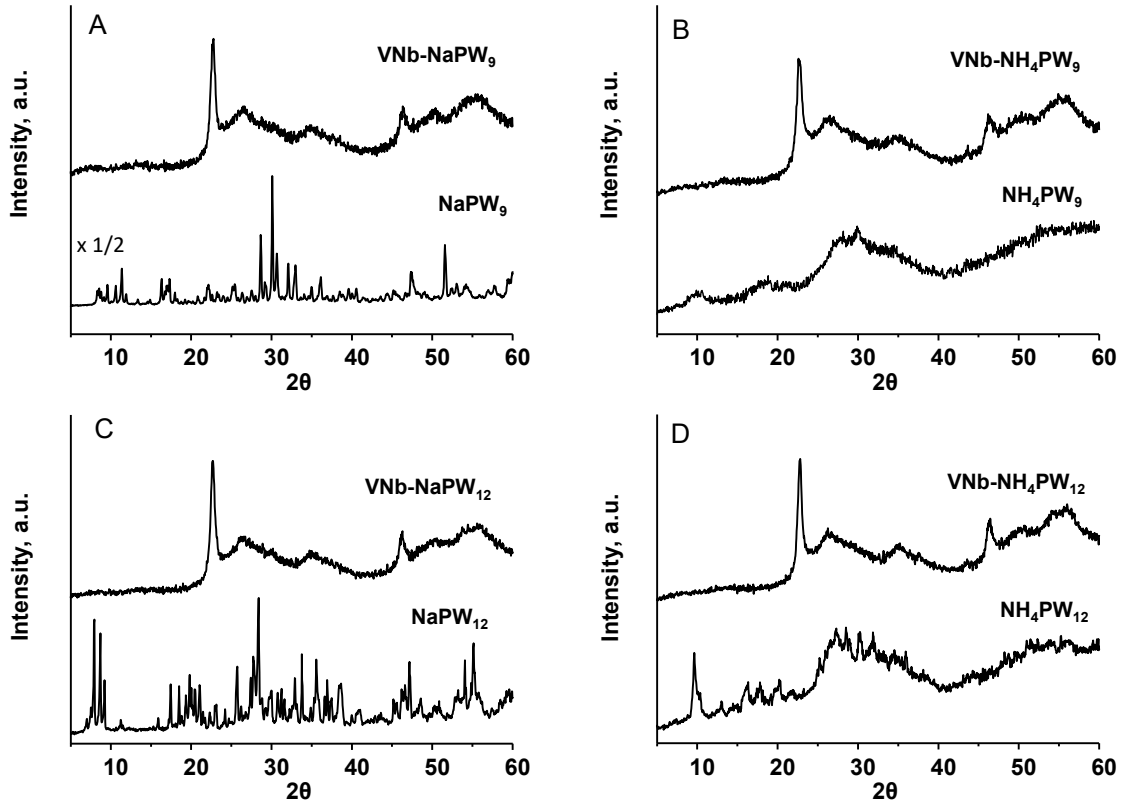

Figure 1. XRD patterns of starting polyoxotungstates (X= $NaPW_9$; NH_4PW_9; $NaPW_{12}$ and NH_4PW_{12}) and the corresponding mixed metal oxides, prepared hydrothermally and heat-treated at 500 ºC (VNb-X series): VNb-$NaPW_9$ (A); VNb-NH_4PW_9 (B); VNb-$NaPW_{12}$ (C); and VNb-NH_4PW_{12} (D).

These diffraction patterns are similar to those achieved for as-synthesized mixed metal oxides samples, i.e. as-VNb-X series (Figs. S1) and as-VNb-MPW_9 (Figs. S2), indicating the conservation of the structure obtained by the hydrothermal synthesis after the heat-treatment at 500 ºC. However, it should be noted that after the subsequent treatment at 800 ºC (in N_2 for 2h) peaks in the range of 2θ = 25-55º (PDF 430390) were similar to those of tetragonal tungsten bronzeTTB [20] suggesting that the material is very orderly (Figure S3, supplementary information). This behavior is similar to that previously reported in other PMoVNbO and PWVNbO bronzes [21-24].

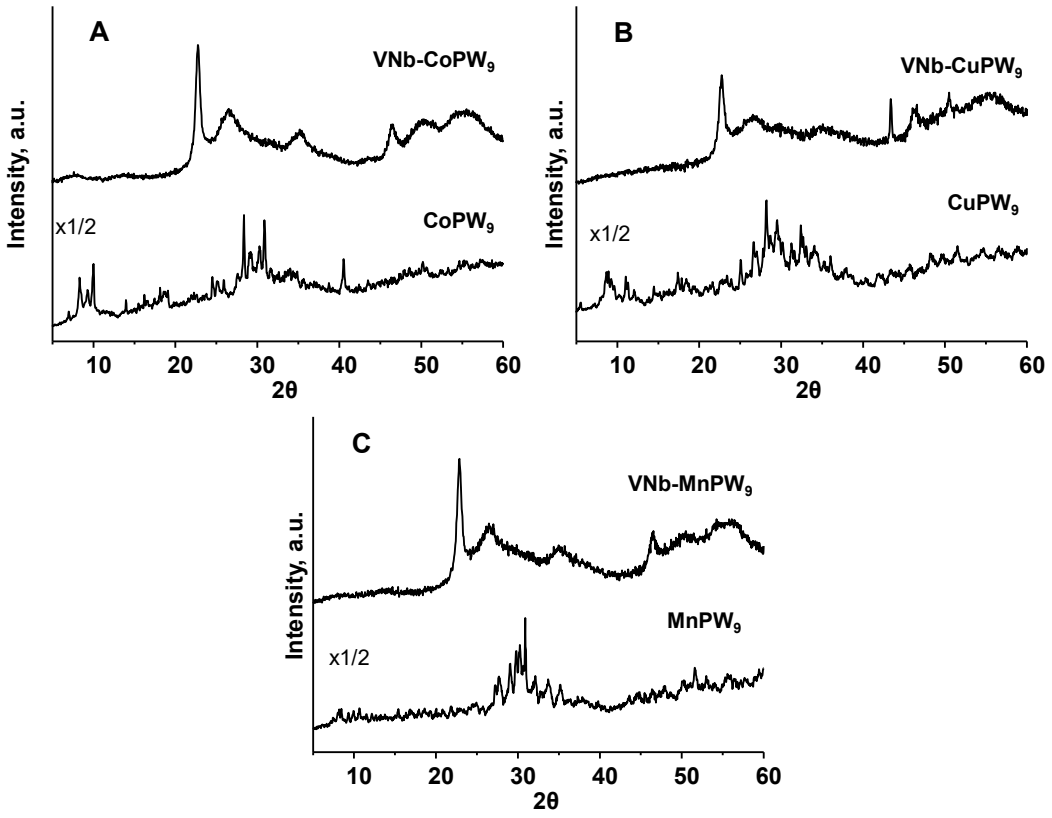

Figure 2. XRD patterns of metal-containing polyoxotungstate (MX= $CoPW_9$, $CuPW_9$ or $MnPW_9$) and the corresponding VNb-containing mixed metal oxides catalysts, prepared hydrothermally and heat-treated at 500 ºC (i.e. VNb-MX series): VNb-$CoPW_9$ (A), VNb-$CuPW_9$ (B) and VNb-$MnPW_9$ (C).

This behavior is similar to that previously reported in other P-Mo-V-Nb-O and P-W-V-Nb-O bronzes [19-22]. In fact, it has been proposed that the incorporation of $V^{(IV)}$ and/or $Nb^{(V)}$ within the framework of tungsten oxide (showing channels of different sizes along the [001] direction) can promote a loss of long-range order in the ab plane of the structure at increasing Nb concentrations in the materials [22]. This loss of periodicity, which observed in both samples heat-treated at 500 ºC (Figs. 1 and 2) and the corresponding as-synthesized samples (Figs. S1 and S2), gives rise to the so-called pseudocrystalline tungsten oxides, ordered just along the c direction (presenting a diffraction line at ca. 2θ = 22.6 to 22.8, depending on the composition of solids).

Figure 3 presents the FTIR (Fig. 3 A) and Raman (Fig. 3 B) spectra of iso and hetero-polyoxotungstates. It is well known that the FTIR spectra of phosphotungstic acid is characterized by the presence of bands at 1080, 983, 893 and 798 cm^{-1} and correspond to P-O, W=O, W-O_{corner}-W and W-O_{edge}-W asymmetric stretching vibrations, respectively [26]. In our cases (Fig. 3A), small differences are observed between samples presenting Keggin structure (i.e. $NaPW_{12}$ and NH_4PW_{12}) and those presenting lacunary Keggin structure (i.e. $NaPW_9$ and NH_4PW_9 and MPW_9, M= Cu, Co or Mn). However, comparison of spectra belonging to the Co/$MnPW_9$ phases and their precursor $NaPW_9$, shows that differences occur in the more sensible region of the heteropolyanion: W=O terminal bonds. Whereas a series of bands appear in the precursor spectrum (992–911 cm^{-1}), only a broad band centered at ~940 cm^{-1} is observed in spectra of condensed phases, in agreement with a low distortion of constitutive polyhedra. Below 900 cm^{-1} the bridged W–O–W bonds do not show appreciable differences, corroborating the stability of condensed WO_6 in the Keggin derivative structure. On the other hand, the W–O–M bond would be associated to the bands located in the lower energy region of spectra

(approximately 500 cm^{-1}) even though the assignment is difficult from this region due to the overlapping of M–O stretching bands with the angular deformations.

Regarding the FTIR spectrum of the Cu phase is different from the rest of its Co and Mn isomers but similar to that of the precursor. As has been discussed and analyzed in our previous works, the preparation of this species involves a mixed of pure $CuPW_9$ with two isomers of Keggin structure ($[Cu_2(H_2O)_2PW_{10}O_{38}]^{7-}$ [17,19] (as thermolysis products) which occurs in the form of two isomers containing neighboring Cu (II) atoms in two different types of bonds (a) connected through oxygen from the vertices of the octahedra and (b) connected through the edges of their coordination octahedral. The FTIR spectrum of $CuPW_9$ clearly shows the splitting of the antisymmetric band of the PO_4 group, (between 1200 and 1000 cm^{-1}) due to the strong distortion of the symmetry of the Keggin isomeric species contained in this phase and caused by the CuO_6 groups. The fact that four bands appear instead of two corroborates the existence of two structural isomers (1139, 1104, 1071, 1038 cm^{-1}). The spectrum (Fig. 3A) comparatively illustrates this behavior by the bands of the precursor $NaPW_9$, of the mixed species of $CuPW_9$ and of the Co /$MnPW_9$ dimers. It is observed that in the range between 1200 and 1000 cm^{-1}, the precursor, being a lacunar species of low symmetry, presents a group of bands corresponding to P-O and P-OH bonds in a distorted environment similar to the $CuPW_9$ phase. In contrast, the other dimeric species present in the same region, a single band belonging to the antisymmetric stretch of the phosphate group of regular tetrahedral symmetry at 1038 cm^{-1}.

It has been suggested that the origin of the decrease in the symmetry of the isomers containing Cu (with $[Cu_2]$) and therefore of the thermal instability of the complex $CuPW_9$ (with $[Cu_4]$) is due to the weak interaction of the CuO_6 octahedra with the P-O bonds of the groups phosphates around which the WO_6 groups are also located. This weak

interaction is possibly caused by the well-known Jahn-Teller distortion in the axial direction typical of the $Cu^{(II)}$ ion in octahedral coordination [17,19]. In this way the phosphate group loses its regular tetrahedral environment and the band of the P-O antisymmetric stretch splits.

The Raman spectra of condensed heteropolyoxometalates (Fig. 3 B) seems to be more simple due to the increase of the general symmetry: a unique line of moderate intensity for the P–O symmetric stretching at ~1050 cm^{-1} and the strongest and sharp line of $W{=}O_t$ symmetric stretching mode at ~970 cm^{-1}. The lines of intermediate intensity at 890 and 820 cm^{-1} can be assigned to the ($W\text{-}O_{corner}\text{-}W$ and $W\text{-}O_{edge}\text{-}W$ vibrations, less affected by condensation effect [17,19].

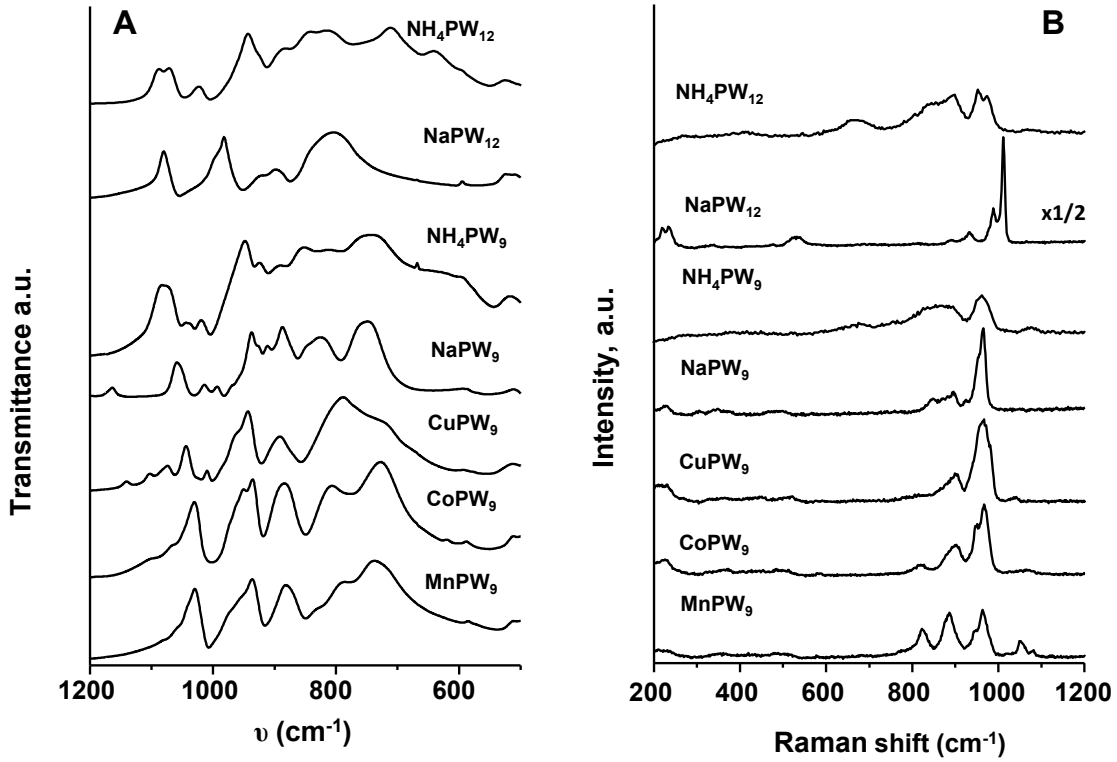

Figure 3. FTIR (A) and Raman (B) spectra of polyoxotungstates: NH_4PW_{12}, $NaPW_{12}$, NH_4PW_9, $NaPW_9$; $CuPW_9$, $CoPW_9$, $MnPW_9$.

Figure 4 presents the FTIR (Fig. 4 A) and Raman (Fig. 4 B) spectra of mixed metal oxides heat-treated at 500 ºC. The infrared spectra obtained for the mixed oxides derived from the PW_9 phase showed an intense band at 795 cm^{-1}, corresponding to the W-O-W bonds of the octahedrons that share edges and V=O and V-O-V vibrations, with a shoulder at 835 cm^{-1}, and another one at 461 cm^{-1} due to deformation modes of the network (M-O-M) [27]. In addition, two much less intense bands were observed at 599 cm^{-1} and 655cm^{-1}, which can be related to deformations of the PO_4 tetrahedral group, and one wide band centered at 1096 cm^{-1} that can be assigned to the stretching modes of P-O-P (1160, 1058 and 1015 cm^{-1}), the band at 1015 cm^{-1} overlapped with the band corresponding to the V=O stretching (1020-1025 cm^{-1}) [22].

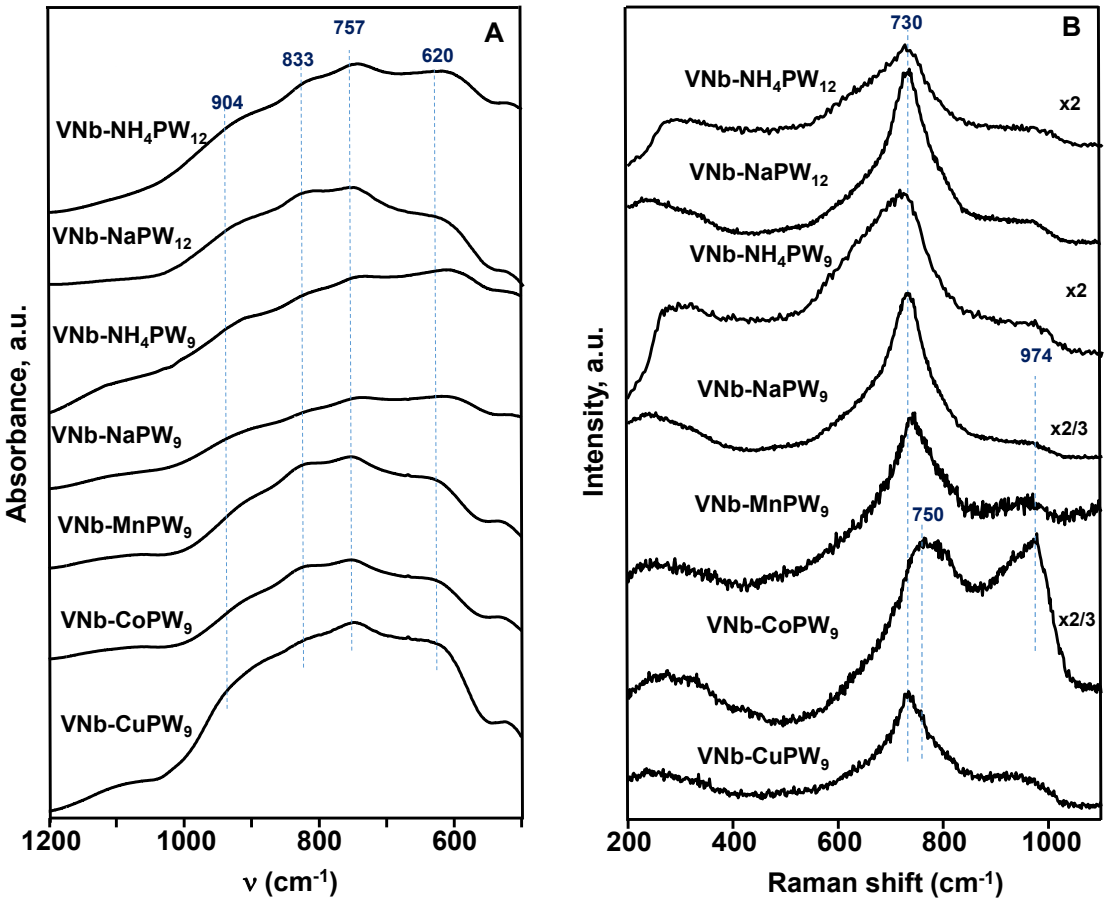

Figure 4. FTIR (A) and Raman (B) spectra of mixed metal oxides heat-treated at 500 ºC (i.e. VNb-X and VNb-MX series): VNb-NH_4PW_{12}, VNb-$NaPW_{12}$, VNb-NH_4PW_9, VNb-$NaPW_9$, VNb-$CuPW_9$, VNb-$CoPW_9$, VNb-$MnPW_9$.

Accordingly, it is possible to make the same assignments for the bands at 466, 797, and 1096 cm^{-1} observed in the infrared spectra of the mixed oxide obtained from the $CuPW_9$ phase and heat-treated at 500 ºC in N_2 (i.e. VNb-$CuPW_9$ catalyst).

Similar conclusion can be proposed from the Raman spectra of heat-treated samples (Fig. 4B). Thus, a broad band at ca 730 cm^{-1} is observed in all cases. It is known that pure tungsten oxide bronze presents a band at ca. 780 cm^{-1}, which can be ascribed to O-W-O stretching vibrations in the MO_6 octahedral framework of a tungsten oxide bronze, whereas bands in the 200-300 cm^{-1} range are related to O–W–O deformation modes [22, 27]. However, the width of this broad band is strongly modified by the incorporation of the other atoms, especially in W-Nb-O mixed oxides [22]. Thus, the band observed at 780 cm^{-1} in pure tungsten oxide bronze progressively shifts to lower values by the incorporation of niobium: i) until ca. 750 cm^{-1} at Nb/W rations lower than 0.5; or ii) to 709 cm^{-1} (band ascribed to the symmetric stretching mode of slightly distorted NbO_6 octahedra in bulk niobium oxides) for samples with higher Nb-contents. Accordingly, a partial substitution of Nb for W can be proposed in our catalysts. In addition, a band at ca. 980 cm^{-1} is also observed for sample VNb-MPW_9 series, which could be related to a higher amount of Me = O species, including $M^{(II)}$ ($M^{(II)}$ = Cu, Co, Mn), in these catalysts.

Figure 5 shows the Diffuse Reflectance UV-vis (DR-UV-vis) spectra of mixed metal oxides heat-treated at 500 ºC. In all cases, it can be seen a broad band at ca. 260 nm. The absence of a band in the 400-500 nm range indicates the absence of pure metal oxides such as V_2O_5 or Nb_2O_5 [28] or WO_3 [29, 30]. However, the assignment of bands in the 200–450 nm range is difficult because the signals of many species converge, i.e. $V^{(V)}$ (250-450 nm) [28], and $Nb^{(V)}$ (235-310 nm) [29]. Moreover, the band at ca. 260 nm can be also assigned to an O→W charge transfer transition as in tungstates and polytungstates

[29, 31, 32] and in W-based bronzes [29, 33] where W is bonded to O in octahedral coordination, especially when considering W-O-Nb and/or W-O-V entities.

In addition, a broad band appears at 620 nm due to d-d transitions of isolated $V^{(IV)}$ species whose intensity depend on the composition of catalyst [28, 34]. However, this band is not observed in the case of VNb-NH_4PW_{12} sample, suggesting that, in this case, vanadium is mainly present as $V^{(V)}$.

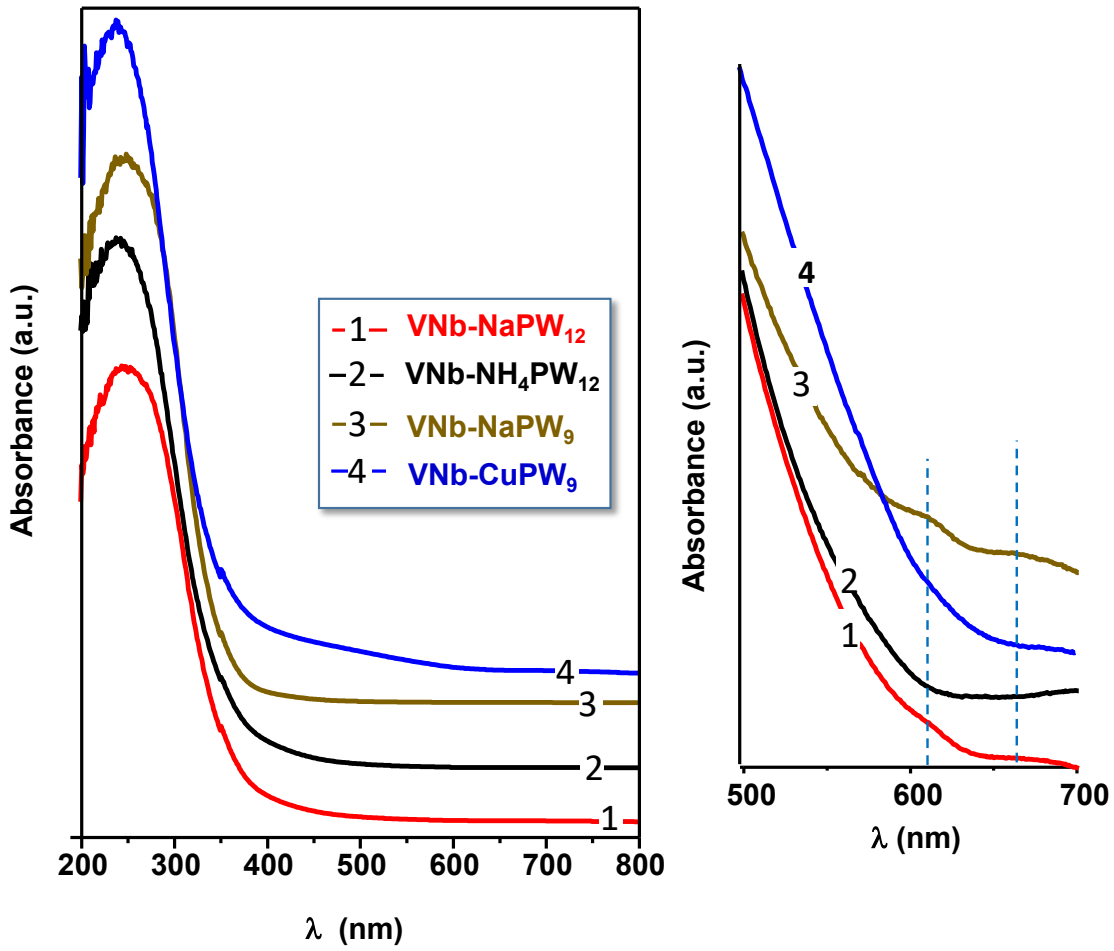

Figure 5. Diffuse reflectance UV–vis spectra of mixed oxides catalysts heat-treated at 500 ºC: VNb-NH_4PW_{12}, VNb-$NaPW_{12}$, VNb-$NaPW_9$ and VNb-$CuPW_9$.

3.2. Catalytic evaluation

Both heteropolyoxometalates and the corresponding mixed metal oxides bronzes (heat-treated at 500 ºC), have been tested in the liquid phase selective oxidation of DPS, in batch at 80 ºC and using toluene as solvent and TBHP as oxidant, and in the gas phase partial oxidation of hydrogen sulfide (H_2S), at atmospheric pressure and using oxygen as oxidant.

3.2.1. Liquid phase selective oxidation of DPS

During the selective oxidation of DPS two reaction products were observed: diphenyl sulfoxide (DPSO) and diphenyl sulfone ($DPSO_2$), being DPSO an intermediate product in the formation of $DPSO_2$. The catalytic test was carried out in a batch reactor with magnetic stirring at 800 rpm, for a good contact surface between catalyst and reaction media, to avoid limitations of mass transfer [11]. Also, considering that all the materials studied presented comparably low surface areas, the catalytic process occurs in the external surface of the solid, so the mass transfer limitation could be avoided [11].

As well, in previous studies, different solvents in the catalytic oxidative process also were analyzed. Acetonitrile allowed to obtain the high performances of oxidation process might be related to its aprotic property (nucleophilic oxidation reaction is performed better in the aprotic solvents with higher dielectric constants) and its low surface tension (facilitate the mass transfer in the reaction). The sulfur-containing compounds exist in the same phase (CH_3CN) whereas the oxidants reside but the catalyst reside in the solid phase. [35,36].

According to previous works, the conversion curves correspond to a reaction rate of the pseudo first order (supplementary information Figure S4). Figures 6 show comparatively the conversion for the starting Keggin phases ($NaPW_9$, NH_4PW_9, $NaPW_{12}$, NH_4PW_{12}) (Fig. 6A), and Me-containing Keggin phases ($CoPW_9$, $CuPW_9$ and $MnPW_9$) (Fig. 6B). The higher catalytic activity was observed for sample $CuPW_9$ (Fig. 6B), which shows a DPS conversion of ca. 80% after 150 min of reaction time.

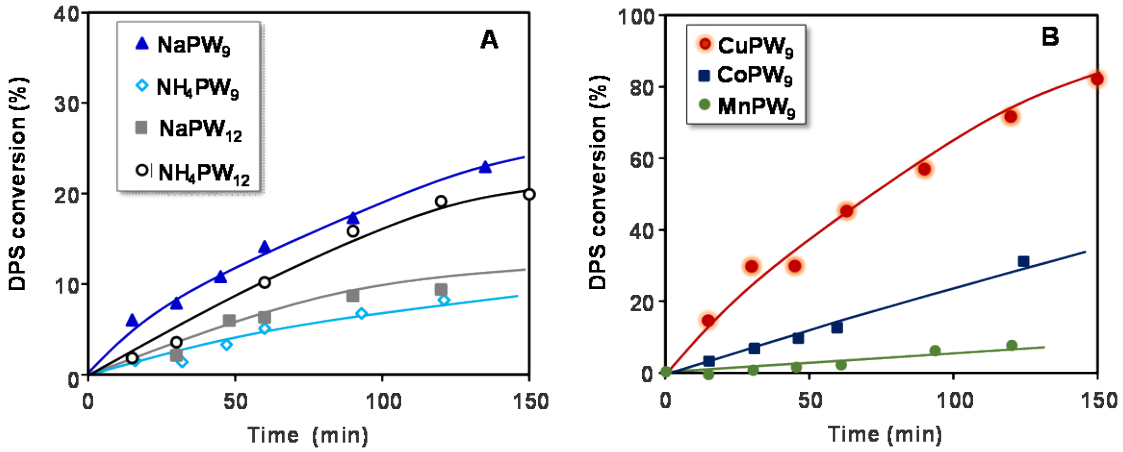

Figure 6. Variation of DPS conversion with reaction time for the Keggin heteropolyoxometalates using 1 mmol % of the catalyst: A) $NaPW_9$; NH_4PW_9; $NaPW_{12}$; and NH_4PW_{12}; and B) $CoPW_9$; $CuPW_9$; and $MnPW_9$. Experimental conditions in text.

On the other hand, no clear influence on catalytic activity can be observed by changing Na^+ by NH_4^+ or between lacunary Keggin PW_9 and the PW_{12} series. In this way, the catalytic activity for DPS conversion decreases in the following order (in parenthesis the DPS conversion at 100 minutes of reaction): $NaPW_9$ (19) > NH_4PW_{12} (16) > $NaPW_{12}$ (10) > NH_4PW_9 (7) (Fig. 6A). Whereas DPS conversion over metal-containing lacunary Keggin decreases in the following trend (in parenthesis the DPS conversion at 100 min of reaction): $CuPW_9$ (62) > $CoPW_9$ (21) > $MnPW_9$ (15) (Fig. 6 B).

Comparison of results obtained with the PW_9 and PW_{12} phases suggests that the activity is related to the chemical properties of the cation present, which plays an important role in defining the activity order. The reactivity is in agreement with the redox potentials for the $M^{(II)}/M$ reduction pair, pointing out the lower copper capacity to remain as divalent species. Contrary, $Mn^{(II)}$ only presents higher oxidation states while $Co^{(II)}$-$Co^{(III)}$ oxidation is relatively difficult in absence of adequate environment. Whereas $Cu^{(II)}$ is the unique species easy to reduce to monovalent ion. On the other hand, the asymmetry of CuO_6 polyhedra by Jahn Teller effect, responsible for the PWCu instability, increases the interaction of the mixture of phases with the reactive and consequently the catalyst activity. Additionally, it is possible to suggest an increase of the $Cu^{(I)}$-sulfide species according to the hard and soft Pearson' acids classification, which can favor the formation of an intermediate meta-stable phase [11].

Figures 7 show comparatively the conversion for the mixed oxides obtained hydrothermally from Keggin phases and heat-treated at 500 ºC. In general, mixed metal oxides bronzes present a catalytic activity for partial oxidation of DPS higher to those achieved over pure polyoxotungstates (Fig. 6).

Thus, mixed metal oxides show conversion values between 80% and 100% at reaction time between 15-30 min, except for Mn- and Co-containing catalysts, which show a lower catalytic activity. Accordingly, the incorporation of $Nb^{(V)}$, but specially $V^{(IV)}$, produces a large increase in conversion in shorter reaction times, suggesting that the presence of these metals should increase the catalytic oxidation power of the mixed oxides.

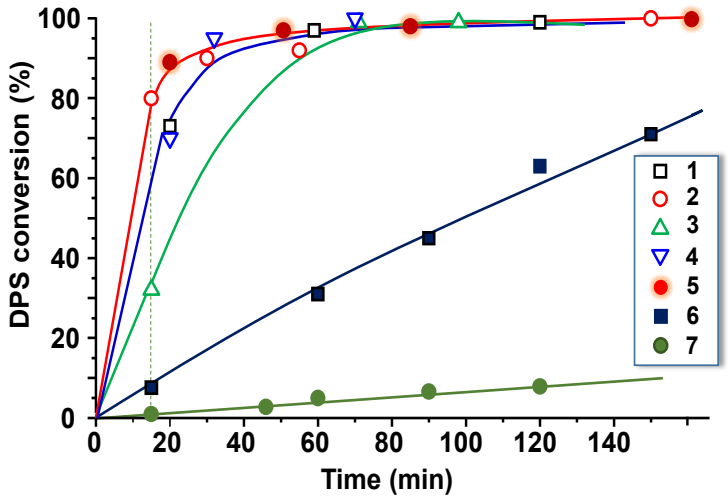

Figure 7. Variation of DPS conversion as function of reaction time obtained over mixed metal oxides, prepared hydrothermally from the Keggin phases, heat-treated at 500 ºC: VNb-$NaPW_9$ (1); VNb-NH_4PW_9 (2); VNb-$NaPW_{12}$ (3); VNb-NH_4PW_{12} (4); VNb-$CuPW_9$ (5); VNb-$CoPW_9$ (6); VNb-$MnPW_9$ (7). Experimental conditions in text.

On the other hand, the nature of Keggin precursor also influences the catalytic performance of mixed metal oxides. In this way, the DPS conversion decreases according to the following trend (in parenthesis the DPS conversion, in %, at reaction time of 15 min): VNb-NH_4PW_9 (80%) = VNb-$CuPW_9$ (80%) > VNb-$NaPW_9$ (58%) = VNb-NH_4PW_{12} (58%) > VNb-$NaPW_{12}$ (32%) > VNb-$CoPW_9$ (7%) > VNb-$MnPW_9$ (2%). Accordingly, mixed metal oxides prepared from lacunary Keggin polyoxometalates are more active than those prepared from Keggin polyoxometalates. In addition, catalysts prepared from Na^+-containing Keggin compounds are more active than those prepared from NH_4^+-containing Keggin polyoxometalate. At this point it is important to note the high activity of the species containing Cu. As has been observed in other previous selective oxidation tests, as mentioned, the reactivity of $Cu^{(II)}$ is evidenced for both the $CuPW_9$ phase and for the VNb-mixed oxide. The previous vibrational, structural and thermal spectrocopic characterization of the species as mentioned before corroborating the manifested reactivity [16-19].

Figure 8 (A and B) shows comparatively the selectivity to DPSO and $DPSO_2$ with the DPS conversion for the $CuPW_9$ Keggin phase (Fig. 8A) and its corresponding mixed metal oxide heat-treated at 500 ºC, i.e. VNb-$CuPW_9$ sample (Fig. 8B). It can be observed that the mixed metal oxide catalyst shows a fast conversion of DPS to $DPSO_2$, whereas the Keggin lacunary sample is more selective to DPSO.

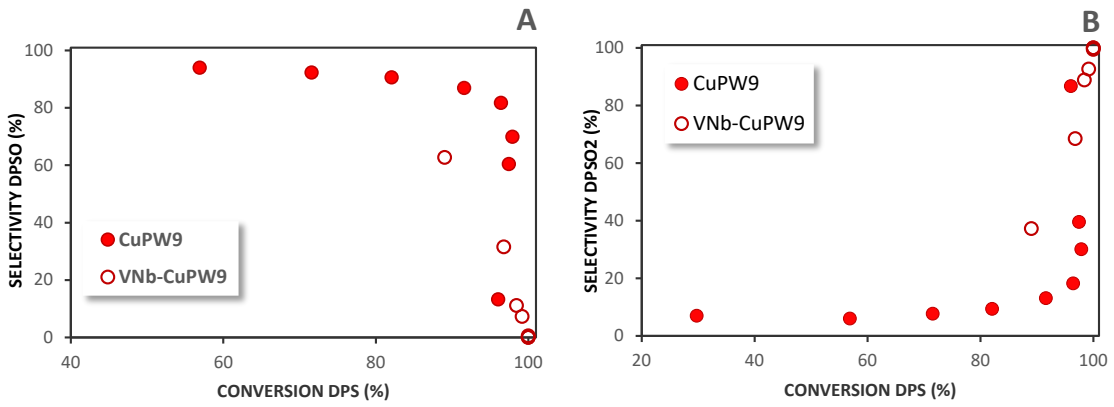

Figure 8. Selectivity to DPSO (A) and $DPSO_2$ (B) with the conversion of DPS in the selective oxidation of DPS over Keggin lacunary $CuPW_9$ and its corresponding mixed metal oxide, VNb-$CuPW_9$. Experimental conditions in text.

For comparative purposes, TOF and TON were evaluated (the calculation were explained in experimental section), for each product under the same conditions (reaction temperature = 80 °C, and time = 150 min) for each of the catalysts (1 mmol%). The values for TON and TOF are presented in Table 2.

Table 2

In fact, it is interesting to note that Keggin-type lacunary phases showed higher DPSO selectivity (DPSO TOF for MPW_9 are higher than those of VNb-MPW_9, table II) up to 100% DPS conversion. However, the corresponding derivative hydrothermal mixed

metal oxide catalyst showed high selectivity to DPSO only at the beginning of the reaction. The selectivity to DPSO was high up to 50% of conversion; then an increase in the selectivity to $DPSO_2$ was observed over mixed metal oxides ($DPSO_2$ TOF for VNb-MPW_9 are higher than those of MPW_9, Table 2).

Accordingly, mixed metal oxides showed a higher selectivity to $DPSO_2$ compared to the starting sandwich phases, due to the incorporation of $Nb^{(V)}$ and $V^{(IV)}$ that introduce both acid and redox active sites, thus obtaining higher catalytic activity and higher selectivity to $DPSO_2$.

We must indicate that a mixed metal oxide without vanadium was evaluated also for comparative purpose. A DPS conversion of 65% after 120 min of reaction was obtained with a high selectivity to DPSO (80%), confirming that $V^{(IV)}$ ion improves the catalytic activity, because it brings redox sites, but improving also the consecutive reaction, i.e. the oxidation of DPSO to $DPSO_2$ process [35].

This behavior of the selectivity of catalyst are according to the plausible mechanism to this reaction that involves the formation of peroxo-tungstate reactive species. It is known that sulfides are oxidized to sulfoxides by electrophilic oxidants. The interaction of peroxide with W catalytic systems (XPW) generates an electrophilic intermediate (peroxo oxygen/metal), which produces an electrophilic attack on the sulfur atom in the sulfide, generating the corresponding sulfoxide. And the mechanism for the oxidation of sulfoxide to the corresponding sulfone involves the formation of a XPW-sulfoxide intermediate through the nucleophilic attack on the tungsten atom in the XPW by the oxygen in the sulfoxide, and then the nucleophilic attack of the sulfur atom in XPW-sulfoxide by TBHP via a SN_2 mechanism [35,36].

On the other hand, the catalytic reuse of sample VNb-$CuPW_9$ was also evaluated. In this case, the conversion decreased by almost half but did not change the selectivity values.

These results are promising and, as expected, the incorporation of $Nb^{(V)}$ and $V^{(IV)}$ metals into the structure introduces acidic and redox sites in the tetragonal bronze precursor giving a bifunctional character to these species, favoring the formation of peroxo-molybdate intermediates and the subsequent nucleophilic attack of the sulfur atom in the sulfide on the peroxo species [36].

3.2.2. Gas phase partial oxidation of hydrogen sulfide

Figure 9 shows the variation of the conversion of H_2S with the time on stream (TOS) during the oxidation of H_2S over heteropolytungstates at 180 ºC (Fig. 9 A) as well as a comparative study of H_2S conversion at 60 and 120 min for all catalysts (Fig. 9 B). For comparison, Figure 10A and Figure 10C) shows comparatively the variation of H_2S conversion with time on stream of the corresponding mixed metal oxides, VNb-X and VNb-MX series, respectively.

Heteropolytungstates present a very low catalytic activity (Fig. 9A and 9B) with respect to those achieved over the corresponding mixed metal oxides bronzes (Fig. 10, A and C). In addition, the conversion of H_2S over metal oxides bronzes strongly depends on the composition of catalysts. Thus, the conversion of H_2S decreases according to the following trend: VNb-$NaPW_{12}$ = VNb-$NaPW_9$ > VNb-$CuPW_9$ > VNb-NH_4PW_{12} = VNb-NH_4PW_9 > VNb-$CoPW_9$ > VNb-$MnPW_9$.

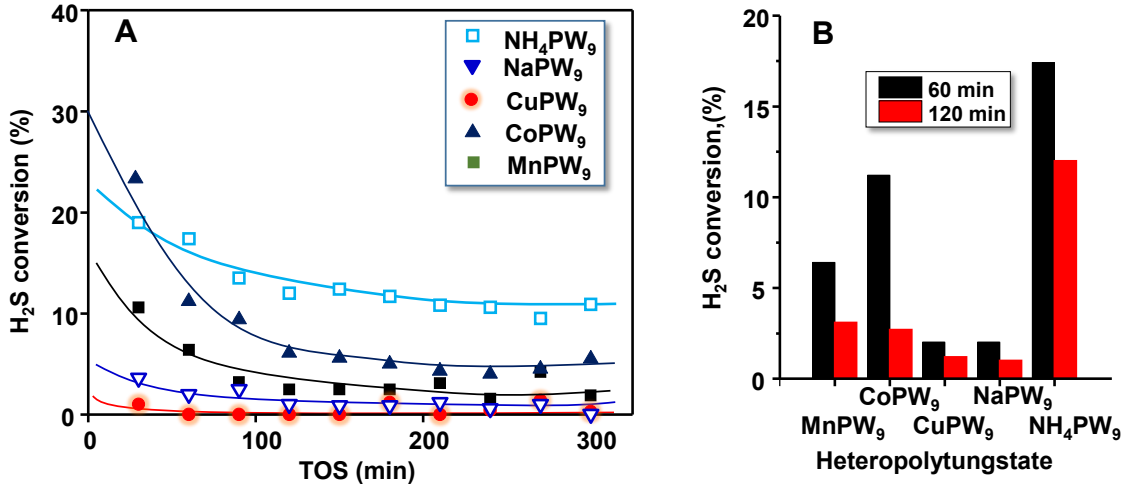

Figure 9. A) Variation of H_2S conversion with time on stream (TOS) during the partial oxidation of H_2S over heteropolytungstates at 180 ºC. B) Catalytic activity for H_2S oxidation at 120 and 60 minutes on heteropolytungstates at 180 ºC. Experimental conditions in text.

On the other hand, we must inform that an important catalyst decay is observed over heteropolytungstates (Fig. 9, A and B). However, a much less important catalyst decay has been observed in the case of mixed oxides bronzes (Fig. 10, A and C). In fact, in the case of mixed oxides bronzes (i.e. VNb-X series) only an initial catalyst decay is observed during the first hours of each experiment. This behavior has been also observed over other metal oxides, i.e. Fe- [37, 38] or V-based catalysts [39, 40], as a consequence of the partial reduction of catalysts during the reaction at a relatively low reaction temperature.

In the case of heteropolytungstates, no important changes in the FTIR spectra are observed when comparing fresh and used catalysts (Fig. S1), which suggests that changes in the catalytic activity with time on stream could be related to a poor redox property of these materials.

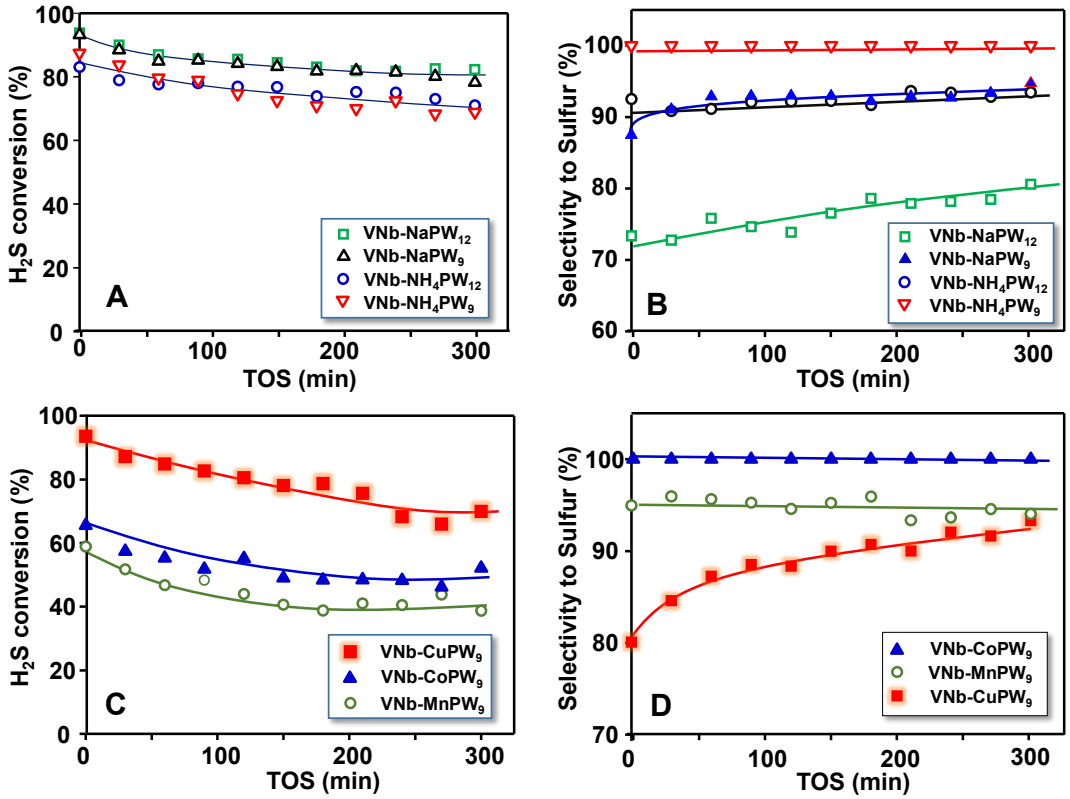

Figure 10. Variation of H_2S conversion (A and C) and the selectivity to sulfur (B and D) with time on stream (TOS) during the partial oxidation of H_2S, at 180 ºC, over mixed metal oxides heat-treated at 500 ºC, i.e. VNb-X and VNb-MX series. (A, B) VNb-$NaPW_{12}$, VNb-NH_4PW_{12}, VNb-$NaPW_9$ and VNb-NH_4PW_9. (C, D) VNb-$CuPW_9$; Nb-$CoPW_9$ and VNb-$MnPW_9$. Experimental conditions in text.

It can be noted that, in all cases, sulfur has been the main reaction products, and only in some cases (especially working at high H_2S conversion) SO_2 was formed as minority (Fig. 10 B and D). In this way, 100% selectivity to sulfur have been observed over heteropolytunsgtates, but this is related to the low conversion of H_2S over these species (Fig. 9).

Some differences in the selectivity to sulfur have been observed, however, in the case of mixed metal oxides. Fig. 10 B and Fig. 10 D shows the variation of the selectivity to sulfur with time on stream over mixed metal oxides. In this way, 100% selectivity to

sulfur have been observed for VNb-NH_4PW_9 (Fig. 10C) and VNb-$CoPW_9$ (Fig. 10 D), however, they are not the more active catalysts (see Figs. 10 A and 10 C, respectively).

Since the selectivity to sulfur strongly depends on the H_2S conversion, Fig. 11 presents the variation of the selectivity to sulfur with the H_2S conversion. According to these results, it can be concluded that VNb-NH_4PW_9 (Fig. 11A) and VNb-$CoPW_9$ (Fig. 11B) are the best catalysts in terms of selectivity to sulfur at H_2S conversion level lower than 80%. At higher H_2S conversion, catalysts VNb-$NaPW_9$ (Fig. 11A) and VNb-$CuPW_9$ (Fig. 11B) presented the higher selectivity to sulfur.

It has been proposed that in Mo- and W-containing catalysts presenting tetragonal tungsten bronze (TTB) structure are active and selective in the partial oxidation of H_2S to sulfur. In this way, Mo-O-V and W-O-V pairs were proposed as the active and selective sites for partial oxidation reaction [21]. In our case, and although the TTB structure is not completely formed, the distribution of elements in the framework of catalysts must be similar. Accordingly, W-O-V and Nb-O-V pairs must be the active and selective in our mixed metal oxides, with V-sites presenting redox properties.

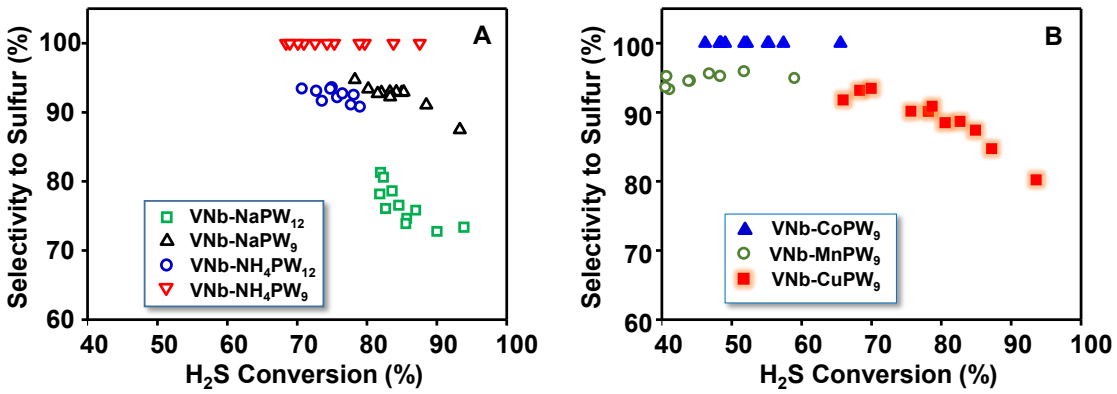

Figure 11. Variation of selectivity to sulfur with H_2S conversion during the partial oxidation of H_2S, at 180 ºC, over mixed metal oxides catalysts, heat-treated at 500 ºC: A) VNb-$NaPW_{12}$, VNb-NH_4PW_{12}, VNb-$NaPW_9$ and VNb-NH_4PW_9; B) VNb-$CuPW_9$, Nb-$CoPW_9$ and VNb-$MnPW_9$. Experimental conditions in text.

4. Conclusions

Using a hydrothermal method, the partial isomorphic substitution of $W^{(VI)}$ by $Nb^{(V)}$ and/or $V^{(IV)}$ in heteropolytungstates derived from a Keggin structure was achieved. The resulting species gave rise to a stable pseudo-crystalline material up to 500 ºC, whereas a tetragonal tungsten bronze structure has been observed when the calcination treatment was continued up to 800 ºC.

Mixed oxides obtained at 500 ºC were evaluated in the selective oxidation of DPS, showing greater activity in shorter reaction times and 100% selectivity to sulfone compared to the starting heteropolycompound. This behavior might be related to $Nb^{(V)}$ incorporation, which modifies the acid characteristics of the hexagonal oxides of tungsten, while the $V^{(IV)}$ introduces new redox sites. Therefore, these materials can be considered as bifunctional catalysts.

Regarding the partial oxidation of H_2S, mixed oxides showed increased activity compared to the starting Heteropolymetalates. However, the catalytic activity for H_2S partial oxidation strongly depended on the redox properties, in which VNb-$NaPW_9$, VNb-$NaPW_{12}$ and VNb-$CuPW_9$ presented the higher H_2S conversion, showing the behavior observed in the DPS reactions. On the other hand, the selectivity to sulfur depended strongly on the level of H_2S conversion achieved. In this way, VNb-NH_4PW_9 and VNb-$CoPW_9$ presents the higher selectivity to sulfur.

Acknowledgment

MGE, MM, CIC and GR thank the financial support by CICPBA Project and UNLP Project 1207. JMLN, MDS and JS thank the financial support by the Spanish Government (Project RTI2018-099668-B-C21).

References

[1] V. C. Srivastava, RSC Advances 2 (2012) 759-783.

[2] K. Sato, M. Hyodo, M. Aoki, X.-Qi Zheng, R. Noyori, Tetrahedron, 57 (2001) 2469-2476.

[3] B. Zapata, F.Pedraza, M.A.Valenzuela, Catal. Today 106 (2005) 219-221.

[4] A. Chica, A. Corma, M.E. Dómine, J. Catal. 242 (2006) 299-308.

[5] Z.Ismagilov, S.Yashnik, M. Kerzhentsev, V. Parmon, A.Bourane, F. M. Al-Shahrani, A.A. Hajji, O.R. Koseoglu, Cat. Rev. - Sci. Eng. 53 (2011) 199-255.

[6] J.M. Campos-Martin, M.C. Capel-Sanchez, P. Perez-Presas, J.L.G. Fierro, J. Chem. Technol. Biotechnol. 85 (2010) 879-890.

[7] D.H. Wang, E.W.H. Qian, H. Amano, K. Okata, A. Ishihara, T. Kabe, Appl. Catal. A Gen. 253 (2003) 91-99.

[8] J.L. García-Gutiérrez, G.C. Laredo, P. García-Gutierrez, F. Jiménez-Cruz, Fuel 138 (2014) 118-125.

[9] J. Lia, Z. Yanga, G. Hub, J. Zhao, Chem. Eng. J. 388 (2020) 124325.

[10] S. Houda, C. Lancelot, P. Blanchard, L. Poinel, C. Lamonier, Catalysts 8 (2018) 344.

[11] a) M. Muñoz, M. G. Egusquiza, I. L. Botto, C. I. Cabello, Current Catal. 3 (2014) 139-146; b) M. G. Egusquiza, K. Ben Tayeb, M. Muñoz, G. Romanelli, C. I. Cabello, I. L. Botto, H. J. Thomas. J. Argentine Chem. Soc. 97 (2009) 166-173.

[12] E. Puello Polo, C. I. Cabello and D. Gazzoli, Current Catalysis 3 (2014) 172-178.

[13] M. Muñoz, M. A. Gallo, A. Gutiérrez-Alejandre, D. Gazzoli, C. I. Cabello, Appl. Catal. B: Environ. 219 (2017) 683–692.

[14] L. Salles, C. Aubry, R. Thouvenot, F. Robert, C. Doremieux-Morin, G. Chottard, H. Ledon, Y. Jeannin, J. Bregeault, Inorg. Chem. 33 (1994) 871-878.

[15] L. Salles, J.Y. Piquemal, R. Thouvenot, C. Minot, J.-M. Brégeault, J. Mol. Catal. A 117 (1997) 375-387.

[16] C. I. Cabello, M. G. Egusquiza, I. L. Botto, G. Minelli, Mat. Chem. Phys. 87 (2004) 264-274.

[17] S. Casuscelli, E. Herrero, M. Crivello, C. Pérez, M. G. Egusquiza, C. I. Cabello, I. L. Botto, Catal. Today 107–108 (2005) 230-234.

[18] M. G. Egusquiza, G. P. Romanelli, C. I. Cabello, I. L. Botto, H. J. Thomas, Catalysis Communications 9 (2008) 45–50.

[19] M. G. Egusquiza, C. I. Cabello, Irma L. Botto, H. J. Thomas, S. Casuscelli, E. Herrero and D. Gazzoli. Catal. Communications, 26 (2012) 117–121.

[20] T. J. R. Weakley, H. T. Evans, J. S. Showell, G. F. Tourné, C. M. Tourné, J. Chem. Soc.Chem. Commun. 1973, 139.

[21] M.D. Soriano, P. Concepción, P. Botella, J.M. López Nieto, Top. Catal. 54 (2011) 729-736.

[22] D. Delgado, P. Concepción, A. Trunschke, J.M. López Nieto, Dalton Trans. 49 (2020) 13282-13293.

[23] P. Botella, B. Solsona, E. García-González, J. M. González-Calbet, J. M. López Nieto, Chem. Commun. 47 (2007) 5040–5042.

[24] N. Blanch-Raga, M.D. Soriano, A.E. Palomares, P. Concepcion, J. Martinez-Triguero, J.M. Lopez Nieto, Appl. Catal. B: Environ. 130–131 (2013) 36– 43.

[25] H. Hayashi, J. B. Moffat, J. Catal. 83 (1983)192-204.

[26] I. V. Kozhevnikov, Catalysis by Polyoxometalates, in Catalysts For Fine Chemicals Synthesis Series, S.M. Roberts, I.V. Kozhevnikov, E. Derouane (Eds.), John Wiley & Sons Ltd., Chichester, England, 2002, vol. 2.

[27] P. Botella, B. Solsona, J. M. López Nieto, P. Concepción, J. L. Jordá, M.T. Doménech-Carbó, Catal. Today 158 (2010) 162-169.

[28] X. Gao, I.E. Wachs, J. Phys. Chem. B 104 (2000) 1261-1268.

[29] E.I. Ross-Medgaarden, I.E. Wachs, J. Phys. Chem. C 111 (2007), 15089-15099.

[30] G.R. Bamwenda, H. Arakawa, Appl. Catal. A: Gen 210 (2001) 181–191.

[31] A. de Lucas, J.L. Valverde, P. Canizares, L. Rodriguez, Appl. Catal. A: Gen 172 (1998) 165–176.

[32] D.G. Barton, M. Shtein, R.D. Wylson, S.L. Soled, E. Iglesia, J. Phys. Chem. B 103 (1999) 630–640.

[33] T. Debnath, S.Ch. Roy, C.H. Ruscher, A. Hussain, J. Mater. Sci. 44 (2009) 179–185.

[34] V.R. Porter, W.B. White, R. Roy, J. Solid State Chem. 4 (1972) 250–254.

[35] A.L. Maciuca, C.E. Ciocan, E. Dumitriu, F. Fajula, V. Hulea. Catal. Today 138 (2008) 33-37.

[36] V. Palermo, G. P. Romanelli, P. Vazquez. J. Mol. Catal. A: Chem. 373 (2013) 142–150.

[37] R. Sanchis, J.A. Cecilia, M.D. Soriano, M.I. Vázquez, A. Dejoz, J.M. López Nieto, E. Rodríguez Castellón, B. Solsona, Chem. Eng. J. 334 (2018) 1159–1168.

[38] R.J.A.M. Terörde, P.J. van den Brink, L.M. Visser, A.J. van Dillen, Catal. Today 17 (1993) 217-224.

[39] M.D. Soriano, J. Jimenez-Jimenez, P. Concepcion, A. Jimenez-Lopez, E. Rodríguez-Castellón, J.M. Lopez Nieto, Appl. Catal. B: Environ. 92 (2009) 271–279

[40] M.I. Kim, D.W. Park, S.W. Park, X. Yang, J.S. Choi, D.J. Suh, Catal. Today 111 (2006) 212–216.

Table 1. S_{BET} data and SEM-EDS chemical analysis (wt %) for Heteropolytungstates and the corresponding mixed metal oxides, prepared hydrothermally and heat-treated at 500ºC.[a]

Catalyst	Type [b]	S_{BET}	Chemical analysis (wt%) by SEM-EDS						
		(m^2 g^{-1})	W	P	Na	M	K	Nb	V
$NaPW_9$	HPT	nd	89.2	5.2	5.6	-	-	-	-
VNb-$NaPW_9$	MMO	152	27.1	0.6	0.1	-	-	72.0	0.2
NH_4PW_9	HPT	nd	86.1	2.6	11.3	-	-	-	-
VNb-NH_4PW_9	MMO		27.8	0.8	-	-	-	70.8	0.6
$NaPW_{12}$	HPT	nd	95.1	1.1	3.8	-	-	-	-
VNb-$NaPW_{12}$	MMO	126	34.9	1.0	0.2	-	-	62.1	1.9
NH_4PW_{12}	HPT	nd	97.8	2.2	-	-	-	-	-
VNb-NH_4PW_{12}	MMO	146	36.0	0.9	-	-	-	60.7	2.5
$CuPW_9$	HPT	nd	82.5	5.1	0.3	7.9	4.2	-	-
VNb-$CuPW_9$	MMO	103	28.7	0.8	0.1	3.9	0.8	63.5	2.2
$CoPW_9$	HPT	nd	63.9	1.4	-	5.1	7.3	-	-
VNb-$CoPW_9$	MMO	64	27.8	2.1	-	9.2	1.5	57.1	2.4
$MnPW_9$	HPT	nd	69.5	0.7	-	4.2	5.6	-	-
VNb-$MnPW_9$	MMO	102	26.2	1.4	-	0.9	0.5	49.7	0.6

a) Type of catalyst: HPT= Heteropolytungstate; MMO= Mixed metal oxide bronzes (prepared hydrothermally and heat-treated at 500 ºC); b) Chemical analysis of both heteropolytungstates (HPT) and mixed metal oxides, (MMO) were carried out by SEM-EDS.

Table 2. Comparison of the effect of catalyst (TON and TOF) for the DPSO and $DPSO_2$ synthesis. [a]

Entry	Catalyst	*TON* (SO)	*TOF* (SO)	*TON* (SO_2)	*TOF* (SO_2)
1	$NaPW_9$	24.4	0.16	1.6	0.01
2	NH_4PW_9	9.0	0.06	0	0
3	NaPW12	10.6	0.07	0.4	0.003
4	NH_4PW_{12}	19.6	0.13	0.4	0.003
5	$CuPW_9$	**74.6**	**0.50**	7.4	0.05
6	$CoPW_9$	33.3	0.22	1.8	0.01
7	$MnPW_9$	12.9	0.09	0.1	0.001
8	VNb-$NaPW_9$	7.0	0.05	93	0.62
9	VNb-NH_4PW_9	6.0	0.04	94	0.63
10	VNb-$NaPW_{12}$	0	0	**100**	**0.67**
11	VNb-NH_4PW_{12}	0	0	**100**	**0.67**
12	VNb-$CuPW_9$	6.9	0.05	9.1	0.06
13	VNb-$CoPW_9$	61.8	0.41	3.3	0.02
14	VNb-$MnPW_9$	7.8	0.05	0.16	0.001

a) Experimental conditions: substrate: 1 mmol; solvent: 5 mL; oxidant: 5 mmol; catalyst 1 mmol %; temperature, 80 °C, time, 150 min; stirring.

Caption to figures

Figure 1. XRD patterns of starting polyoxotungstates (X= $NaPW_9$; NH_4PW_9; $NaPW_{12}$ and NH_4PW_{12}) and the corresponding mixed metal oxides, prepared hydrothermally and heat-treated at 500 ºC (VNb-X series): VNb-$NaPW_9$ (A); VNb-NH_4PW_9 (B); VNb-$NaPW_{12}$ (C); and VNb-NH_4PW_{12} (D).

Figure 2. XRD patterns of metal-containing polyoxotungstate (MX= $CoPW_9$, $CuPW_9$ or $MnPW_9$) and the corresponding VNb-containing mixed metal oxides catalysts, prepared hydrothermally and heat-treated at 500 ºC (i.e. VNb-MX series): VNb-$CoPW_9$ (A), VNb-$CuPW_9$ (B) and VNb-$MnPW_9$ (C).

Figure 3. FTIR (A) and Raman (B) spectra of polyoxotungstates: NH_4PW_{12}, $NaPW_{12}$, NH_4PW_9, $NaPW_9$; $CuPW_9$, $CoPW_9$, $MnPW_9$.

Figure 4. FTIR (A) and Raman (B) spectra of mixed metal oxides heat-treated at 500 ºC (i.e. VNb-X and VNb-MX series): VNb-NH_4PW_{12}, VNb-$NaPW_{12}$, VNb-NH_4PW_9, VNb-$NaPW_9$, VNb-$CuPW_9$, VNb-$CoPW_9$, VNb-$MnPW_9$.

Figure 5. Diffuse reflectance UV–vis spectra of mixed oxides catalysts heat-treated at 500 ºC: VNb-NH_4PW_{12}, VNb-$NaPW_{12}$, VNb-$NaPW_9$ and VNb-$CuPW_9$.

Figure 6. Variation of DPS conversion with reaction time for the Keggin heteropolyoxometalates: A) $NaPW_9$, NH_4PW_9, $NaPW_{12}$, NH_4PW_{12}; and B) $CoPW_9$, $CuPW_9$ and $MnPW_9$. Experimental conditions in text.

Figure 7. Variation of DPS conversion as function of reaction time obtained over mixed metal oxides, prepared hydrothermally from the Keggin phases, heat-treated at 500 ºC: VNb-$NaPW_9$ (1); VNb-NH_4PW_9 (2); VNb-$NaPW_{12}$ (3); VNb-NH_4PW_{12} (4); VNb-$CuPW_9$ (5); VNb-$CoPW_9$ (6); VNb-$MnPW_9$ (7). Experimental conditions in text.

Figure 8. **S**electivity to DPSO (A) and $DPSO_2$ (B) with the conversion of DPS in the selective oxidation of DPS over Keggin lacunary $CuPW_9$ and its corresponding mixed metal oxide, VNb-$CuPW_9$. Experimental conditions in text..

Figure 9. A) Variation of H_2S conversion with time on stream (TOS) during the partial oxidation of H_2S over heteropolytungstates at 180 ºC. B) Catalytic activity for H_2S oxidation at 120 and 60 minutes on heteropolytungstates at 180 ºC. Experimental conditions in text.

Figure 10. Variation of H_2S conversion (A and C) and the selectivity to sulfur (B and D) with time on stream (TOS) during the partial oxidation of H_2S, at 180 ºC, over mixed metal oxides heat-treated at 500 ºC, i.e. VNb-X and VNb-MX series. (A, B) VNb-$NaPW_{12}$, VNb-NH_4PW_{12}, VNb-$NaPW_9$ and VNb-NH_4PW_9. (C, D) VNb-$CuPW_9$; Nb-$CoPW_9$ and VNb-$MnPW_9$. Experimental conditions in text.

Figure 11. Variation of selectivity to sulfur with H_2S conversion during the partial oxidation of H_2S, at 180 ºC, over mixed metal oxides catalysts, heat-treated at 500 ºC: A) VNb-$NaPW_{12}$, VNb-NH_4PW_{12}, VNb-$NaPW_9$ and VNb-NH_4PW_9; B) VNb-$CuPW_9$, Nb-$CoPW_9$ and VNb-$MnPW_9$. Experimental conditions in text.

Graphical abstract